Real-time cancellation of temperature induced resonance shifts in SOI wire waveguide ring resonator label-free biosensor arrays

D.-X. Xu,[1,*] M. Vachon,[1] A. Densmore,[1] R. Ma,[1] S. Janz,[1] A. Delâge,[1] J. Lapointe[1], P. Cheben,[1] J. H. Schmid,[1] E. Post,[1] Sonia Messaoudène,[2] and Jean-Marc Fédéli [2]

[1]Institute for Microstructural Sciences, National Research Council Canada, 1200 Montreal Rd., Ottawa, Ontario, K1A 0R6 Canada,

[2] CEA, LETI, Minatec, CEA-Grenoble, 17 rue des Martyrs, F-38054 GRENOBLE Cedex 9, France.

**Danxia.Xu@nrc-cnrc.gc.ca*

Abstract: A comprehensive investigation of real-time temperature-induced resonance shift cancellation for silicon wire based biosensor arrays is reported for the first time. A reference resonator, protected by either a SU8 or SiO_2 cladding layer, is used to track temperature changes. The temperature dependence of resonators in aqueous solutions, pertinent to biosensing applications, is measured under steady-state conditions and the operating parameters influencing these properties are discussed. Real-time measurements show that the reference resonator resonances reflect the temperature changes without noticeable time delay, enabling effective cancellation of temperature-induced shifts. Binding between complementary IgG protein pairs is monitored over 4 orders of magnitude dynamic range down to a concentration of 20 pM, demonstrating a resolvable mass of 40 attograms. Reactions are measured over time periods as long as 3 hours with high stability, showing a scatter corresponding to a fluid refractive index fluctuation of $\pm$ 4 $\times$ 10^{-6} in the baseline data. Sensor arrays with a SU8 protective cladding are easy to fabricate, while oxide cladding is found to provide superior stability for measurements involving long time scales.

OCIS codes: (130.3120) Integrated optics devices; (220.0220) Optical design and fabrication; (230.5750) Resonators; (130.6010) Sensors; (120.0120) Instrumentation, measurement, and metrology

References and links

1. K. Tiefenthaler, and W. Lukosz, "Sensitivity of grating couplers as integrated-optical chemical sensors," J. Opt. Soc. Am. B **6**(2), 209–220 (1989).
2. B. Luff, J. Wilkinson, J. Piehler, U. Hollenbach, J. Ingenhoff, and N. Fabricius, ""Integrated optical Mach-Zehnder biosensor," Lightwave Technology," Journalism **16**, 583–592 (1998).
3. R. Heideman, R. Kooyman, and J. Greve, "Performance of a highly sensitive optical waveguide Mach-Zehnder interferometer immunosensor," Sens. Actuators B Chem. **10**(3), 209–217 (1993).
4. F. Prieto, B. Sepulveda, A. Calle, A. Llobera, C. Dominguez, and L. Lechuga, "Integrated Mach-Zehnder interferometer based on ARROW structures for biosensor applications," Sens. Actuators B Chem. **92**(1-2), 151–158 (2003).
5. J. Homola, S. Yee, and G. Gauglitz, "Surface plasmon resonance sensors: review," Sens. Actuators B Chem. **54**(1-2), 3–15 (1999).
6. R. Karlsson, "SPR for molecular interaction analysis: a review of emerging application areas," J. Mol. Recognit. **17**(3), 151–161 (2004).
7. A. Densmore, D.-X. Xu, P. Waldron, S. Janz, P. Cheben, J. Lapointe, A. Delâge, B. Lamontagne, J. Schmid, and E. Post, "A silicon-on-insulator photonic wire based evanescent field sensor," IEEE Photon. Technol. Lett. **18**(23), 2520–2522 (2006).
8. D.-X. Xu, A. Densmore, A. Delâge, P. Waldron, R. McKinnon, S. Janz, J. Lapointe, G. Lopinski, T. Mischki, E. Post, P. Cheben, and J. H. Schmid, "Folded cavity SOI microring sensors for high sensitivity and real time measurement of biomolecular binding," Opt. Express **16**(19), 15137–15148 (2008).
9. A. L. Washburn, L. C. Gunn, and R. C. Bailey, "Label-free quantitation of a cancer biomarker in complex media using silicon photonic microring resonators," Anal. Chem. **81**(22), 9499–9506 (2009).

#133293 - $15.00 USD Received 11 Aug 2010; revised 6 Oct 2010; accepted 6 Oct 2010; published 13 Oct 2010

10. K. De Vos, I. Bartolozzi, E. Schacht, P. Bienstman, and R. Baets, "Silicon-on-Insulator microring resonator for sensitive and label-free biosensing," Opt. Express **15**(12), 7610–7615 (2007).
11. A. Yalcin, K. Popat, J. Aldridge, T. Desai, J. Hryniewicz, N. Chbouki, B. Little, O. King, V. Van, and S. Chu, D. Gill, M. Anthes-Washburn, M. S. Unlu, and B. B. Goldberg "Optical sensing of biomolecules using microring resonators," IEEE J. Sel. Top. Quantum Electron. **12**(1), 148–155 (2006).
12. A. Densmore, M. Vachon, D.-X. Xu, S. Janz, R. Ma, Y.-H. Li, G. Lopinski, A. Delâge, J. Lapointe, C. C. Luebbert, Q. Y. Liu, P. Cheben, and J. H. Schmid, "Silicon photonic wire biosensor array for multiplexed real-time and label-free molecular detection," Opt. Lett. **34**(23), 3598–3600 (2009).
13. K. De Vos, J. Girones, T. Claes, Y. De Koninck, S. Popelka, E. Schacht, R. Baets, and P. Bienstman, "Multiplexed antibody detection with an array of silicon-on-insulator microring resonators," IEEE Photonics J. **1**(4), 225–235 (2009).
14. M. Iqbal, M. Gleeson, B. Spaugh, F. Tybor, W. Gunn, M. Hochberg, T. Baehr-Jones, R. Bailey, and L. Gunn, "Label-Free Biosensor Arrays Based on Silicon Ring Resonators and High-Speed Optical Scanning Instrumentation," IEEE J. Sel. Top. Quantum Electron. **16**(3), 654–661 (2010).
15. D.-X. Xu, M. Vachon, A. Densmore, R. Ma, A. Delâge, S. Janz, J. Lapointe, Y. Li, G. Lopinski, D. Zhang, Q. Y. Liu, P. Cheben, and J. H. Schmid, "Label-free biosensor array based on silicon-on-insulator ring resonators addressed using a WDM approach," Opt. Lett. **35**(16), 2771–2773 (2010).
16. J. H. Schmid, W. Sinclair, J. García, S. Janz, J. Lapointe, D. Poitras, Y. Li, T. Mischki, G. Lopinski, P. Cheben, A. Delâge, A. Densmore, P. Waldron, and D.-X. Xu, "Silicon-on-insulator guided mode resonant grating for evanescent field molecular sensing," Opt. Express **17**(20), 18371–18380 (2009).
17. N. Jokerst, M. Royal, S. Palit, L. Luan, S. Dhar, and T. Tyler, "Chip scale integrated microresonator sensing systems," J Biophotonics **2**(4), 212–226 (2009).
18. S. Chu, B. Little, W. Pan, T. Kaneko, S. Sato, and Y. Kokubun, "An eight-channel add-drop filter using vertically coupled microring resonators over a cross grid," IEEE Photon. Technol. Lett. **11**(6), 691–693 (1999).
19. J. Lee, D. Kim, H. Ahn, S. Park, and G. Kim, "Temperature dependence of silicon nanophotonic ring resonator with a polymeric overlayer," J. Lightwave Technol. **25**(8), 2236–2243 (2007).
20. W. Ye, J. Michel, and L. Kimerling, "Athermal high-index-contrast waveguide design," IEEE Photon. Technol. Lett. **20**(11), 885–887 (2008).
21. K. B. Gylfason, C. F. Carlborg, A. Kaźmierczak, F. Dortu, H. Sohlström, L. Vivien, C. A. Barrios, W. van der Wijngaart, and G. Stemme, "On-chip temperature compensation in an integrated slot-waveguide ring resonator refractive index sensor array," Opt. Express **18**(4), 3226–3237 (2010).
22. M.-S. Kwon, and W. H. Steier, "Microring-resonator-based sensor measuring both the concentration and temperature of a solution," Opt. Express **16**(13), 9372–9377 (2008).
23. H.-S. Lee, G.-D. Kim, and S.-S. Lee, "Temperature Compensated Refractometric Biosensor Exploiting Ring Resonators," IEEE Photon. Technol. Lett. **21**(16), 1136–1138 (2009).
24. E. Palik, *Handbook of optical constants of solids II* (Academic press, 1991).
25. G. Cocorullo, F. Della Corte, and I. Rendina, "Temperature dependence of the thermo-optic coefficient in crystalline silicon between room temperature and 550 K at the wavelength of 1523 nm," Appl. Phys. Lett. **74**(22), 3338 (1999).
26. H. El-Kashef, "The necessary requirements imposed on polar dielectric laser dye solvents–II," Physica B **311**(3-4), 376–379 (2002).
27. J. Stepánek, H. Vaisocherová, and M. Piliarik, eds., *Molecular Interactions in SPR Sensors* (Springer, 2006).

1. Introduction

Evanescent field (EVF) waveguide sensors detect changes in its ambient refractive index by monitoring the associated phase changes. This class of sensors has been used in a range of applications, specifically in monitoring the binding between biomolecules such as proteins and DNA oligos [1–5]. EVF sensors can provide information on the presence and concentration of target molecules without the cumbersome procedure of labeling the target molecules, i.e. label-free detection. The reactions can be monitored in real-time, providing kinetic information crucial for the understanding of molecular interaction and the development of new medical treatment procedures [6]. Surface plasmon resonance (SPR) is a commercially established EVF sensing technology based on bulk-optics. SPR instruments tend to be large and high cost because they require mechanical and temperature stabilization [5]. There has been a continued effort for the past two decades to use planar waveguides as EVF sensing transducers [1–4]. Planar waveguide EVF sensors provide significant size reduction and they are amendable to integration for more robust operation and multiplexed analysis with high channel count assays. Recently EVF sensors based on high index contrast materials such as silicon-on-insulator (SOI) [7–10], silicon nitride and doped silica glass waveguides [4,11] have seen rapid development. Silicon wires are particularly sensitive to surface adsorption since the optical modal electric field can be strongly localized near the waveguide surface due to the high refractive index of silicon [7]. Highly compact SOI sensor

#133293 - $15.00 USD Received 11 Aug 2010; revised 6 Oct 2010; accepted 6 Oct 2010; published 13 Oct 2010

arrays are readily manufacturable using standard CMOS processing [12–15]. Among different types of transducers which convert a phase change into an easily measurable intensity variation, ring resonators provide high sensitivity since the light circulating in the ring effectively interacts with the same molecules many times [16,17]. These properties make silicon wire based resonators one of the most promising sensor platforms.

Practical instruments for assay and molecular binding measurements must be robust and immune to external environmental changes. One of the most commonly encountered problems is temperature drift. As with many other sensors, the high sensitivity of a silicon photonic wire ring resonator to captured molecules also comes at the cost of a high sensitivity to temperature. The temperature can be actively controlled and stabilized as is done in some commercial SPR instruments, which stabilize the temperature to ± 0.01°C. This method is effective but it inevitably adds to the instrument size and cost. For planar waveguide sensors, there are several possibilities to implement on-chip temperature-induced signal drift cancellation. The first is to make the transducers athermal using core and cladding materials with opposite signs in their thermo-optic (TO) constants [18–20]. The waveguide cross-section can be tailored to control the fraction of power in the constituent materials, achieving athermal performance. The use of this method is limited by constraints such as the choice of cladding materials. Specifically, the sensor upper cladding must be an aqueous solution for most biosensing applications. Another method is to use a resonator as the reference which is otherwise identical to the surface sensing elements, but placed in a dedicated fluidic channel with running buffer solutions. The signal difference between the sensing and reference transducer elements in the analyte and buffer solutions gives the corrected sensing signal [21]. This method assumes that the buffer and analyte solutions have the same refractive indices and they are at the same temperature at all times, which is difficult to ensure in practice. Yet another method, which we investigate in this work, is to place a reference ring in the same fluidic channel as the sensing elements. The reference ring is protected by a cladding layer sufficiently thick to optically isolate the waveguides from the sensing medium. The question is whether the reference resonator can simultaneously maintain good thermal contact with the sensing medium.

The use of a reference resonator to monitor temperature changes has been proposed in other publications on SOI resonator sensor arrays [14,15]. However, detailed device structures or operation requirements have not yet been reported. A similar approach has been investigated for polymer waveguide sensors, but the measurements were taken by dipping the sensors in bulk fluids and only provided steady-state information [22,23]. In this work, we study the properties of reference resonators protected by two types of cladding materials, i.e. SU8 polymer and silicon dioxide (SiO_2). Steady-state and real-time measurements were carried out using a microfluidic channel. We show that for the time scales of temperature variants typical in most sensing applications, the reference and sensing resonators experience the same thermal environment, allowing accurate real-time temperature drift cancellation on-chip. Sensing experiments using both sucrose solutions and immunoglobulin G (IgG) proteins demonstrate high sensitivity and uniformity of silicon wire sensor arrays.

2. Sensor array fabrication and temperature-induced resonance shift under steady-state

We first investigate the factors influencing the resonator temperature dependence under steady-state conditions. Serially coupled resonator arrays containing one reference ring and one to four sensing rings are used in the experiment, as schematically shown in Fig. 1a. The reference ring is protected by a 2 μm thick upper cladding layer and optically isolated from the sensing medium, while it resides in the same fluidic channel as the sensing rings. Through experiments we will verify whether the reference and sensing rings are at the same temperature. All the resonators have the same directional coupler of 3 μm long with a gap of 0.5 μm. The reference ring has a radius of 20 μm, and the radii for the sensing rings range from 22 μm to 28 μm with an increment of 2 μm from each other. The resonance wavelengths from each sensor are separated by approximately 1 nm, and the sensors are addressed using wavelength division multiplexing (WDM) [15]. Although serially coupled resonators are used

#133293 - $15.00 USD Received 11 Aug 2010; revised 6 Oct 2010; accepted 6 Oct 2010; published 13 Oct 2010

in this study, the conclusions on the resonator temperature dependence and its cancellation are also applicable for other sensor array configurations such as power broadcasting [12–14].

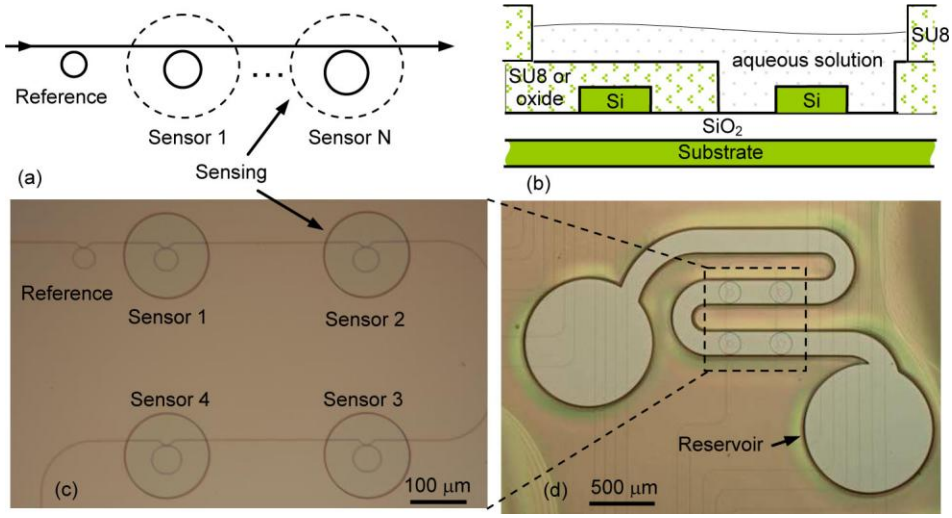

Fig. 1. (a) Schematic of the ring resonator sensor array with a reference ring for tracking sensor temperature changes. The reference is protected by a2 μm thick SU8 or SiO_2 cladding layer. The resonators are coupled in series and addressed using WDM; (b) Schematic of the device cross-section; (c) Fabricated sensor array with one reference and four sensing resonators; (d) Sensor array integrated with a microfluidic channel made in a SU8 film.

The ring and access waveguides have a nominal cross-section of 450 nm × 260 nm and are designed to operate in the quasi-TM fundamental mode for enhanced sensing response [7]. The fabrication process and inverse taper mode size converters used at the facets have been reported previously [8]. After waveguide patterning, a protective cladding layer of 2 μm thick was deposited on the entire chip. Windows approximately 170 μm wide were then opened in this film to expose the sensing resonators. Finally a microfluidic channel was formed on-chip using a 50 μm thick SU8 layer, and delivered the same sensing fluid to the reference and the sensing rings [12].

Two types of protective cladding materials, i.e. SU8 polymer (type A) and SiO_2 (type B) are investigated. SU8 polymer is a commonly used material in microfabrication and it can be patterned by photolithography, therefore the fabrication process is straightforward. For type A samples, sensing windows were opened over the active area in the 2 μm thick SU8 layer using optical contact lithography. The chips were then baked at 200 °C for 60 minutes to cure the film. Finally, samples were exposed to an O_2 plasma to remove any residual organics in the sensor windows as well as to oxidize the silicon surface to form the desired oxide layer of approximately 3 nm in thickness to assist surface functionalization procedures. The substrates were from off the shelf Unibond wafers with a nominal silicon thickness of 260 nm, but the actual thickness was not measured. Waveguides on type A samples were patterned using electron-beam lithography at the National Research Council Canada.

Oxide (SiO_2) is a well known passivation material, however the process of opening the sensing windows is more difficult due to a poor dry-etch selectivity between silicon and SiO_2. To improve fabrication tolerances in type B samples, a thin layer of silicon nitride is embedded in the upper cladding 200 nm above the silicon surface as an etch-stop, and the total cladding layer thickness is ~2 μm. All dielectric layers were deposited using plasma-enhanced chemical vapor deposition (PECVD), and the top thick SiO_2 layer was deposited using tetraethyl orthosilicate (TEOS) as the reaction precursor. The starting SOI wafers had a silicon thickness of 340 nm. Thermal oxidation was used to reduce the Si thickness to the 260 nm target, and the process was monitored using ellipsometry. Waveguides on type B samples were patterned using 193 nm DUV lithography at CEA-LETI. Since type A and B samples

#133293 - $15.00 USD Received 11 Aug 2010; revised 6 Oct 2010; accepted 6 Oct 2010; published 13 Oct 2010

were made from different batches of SOI wafers, required different processing steps and were made in different facilities, small variations in waveguide height and width are expected.

The optical testing was performed using a tunable laser, coupled to the waveguide input facet via a polarization maintaining lensed fiber. The output light was collected and focused onto a photodetector using a 20 × microscope objective lens. Each transmission spectrum takes approximately 6 seconds to acquire when using 1 pm scan steps. The temperature dependence of the resonance wavelength $\partial\lambda/\partial T$ under equilibrium conditions was obtained by measuring the resonances at temperatures from 25 °C to 35 °C. The sample stage temperature was adjusted using a thin film heater and a controller with a resistance temperature detector (RTD) embedded in the copper block between the heater and the sample. When measuring sensor response with water as the test fluid, the liquid was drawn through the fluidic channel and delivered to the sensors at a flow rate of 2 mL/hour, and then the flow was reduced to 0.2 mL/hour while the temperature is stabilized for each setting. The slow flow was maintained to avoid air bubbles forming around the waveguides that can lead to skewed results.

Figure 2(a) shows the transmission spectra of one reference (SiO_2 cladding) and one sensing (in water) ring from a type B sample immersed in water at several steady-state temperatures. Repeated measurements taken at each temperature exhibit high reproducibility with a data variation of less than ± 0.5 pm, as shown in Fig. 2(b). The same data are plotted as a function of temperature in Fig. 2(c), and the values of $\partial\lambda/\partial T$ for both the reference and sensing rings are extracted at these wavelengths (λ ~1535 nm). The results for both type A and B samples with and without water in the fluidic channel are shown in Fig. 2(d) as a function of wavelength. The results for λ = 1550 nm are summarized in Table 1. The waveguide group index $n_g = \lambda^2/(FSR \cdot L)$ is also listed in the table, extracted from the resonator free spectral range (FSR). Here L is the resonator cavity circumference. For each type of sample, the same device is used in the measurements with the sample exposed to air or immersed in water in order to ensure the same waveguide dimensions.

To better understand the observed results, simulations are carried out using a full vectorial mode solver (Fimmwave) to calculate the waveguide effective index n_{eff} and group index n_g at different temperatures. The properties of the relevant materials are listed in Table 2, where the refractive index of SU8 in the wavelength range of 633 nm to 1620 nm is obtained using variable angle spectroscopic ellipsometry. The material dispersion is included in the simulations. For a ring resonator sensor, $\partial\lambda/\partial T$ can be expressed as:

$$\frac{\partial \lambda}{\partial T} = \frac{\lambda}{n_g} \frac{\partial n_{eff}}{\partial T} \tag{1}$$

For comparison with experiments, we first simulate $\partial\lambda/\partial T$ and n_g for a resonator with the nominal cross-section of 450 nm × 260 nm. The results for air, water and SiO_2 claddings are listed in Table 1 and compared with measured results of a type B sample. For all three cladding materials, the simulated and measured results are in general agreement. The larger calculated values in n_g suggest that the fabricated waveguides have a smaller cross-section.

We then tried to match the measurements of the type A sample in air, since this is the case with the best known material constants. A cross-section of 450 nm × 240 nm gives the closest agreement in both $\partial\lambda/\partial T$ and n_g (Table 1). Using the same waveguide size, simulations were also performed for water and SU8 upper claddings, and the results are in agreement with measurements. These results indicate that the waveguides in the type A samples are even smaller than the nominal size. In reality, the size difference is likely to be in both the waveguide width and height. Since these waveguides operate in the TM polarization, the optical properties depend on the waveguide height more strongly than on the width. If assuming a waveguide height of 260 nm, a width of < 350 nm would be required to match the measured values, and that is inconsistent with sample inspection observations. Lastly, the material constants are taken from bulk values and they may not be identical to the values for thin films encountered in these experiments. This can also contribute to the small discrepancies between the theory and experiments.

#133293 - $15.00 USD Received 11 Aug 2010; revised 6 Oct 2010; accepted 6 Oct 2010; published 13 Oct 2010

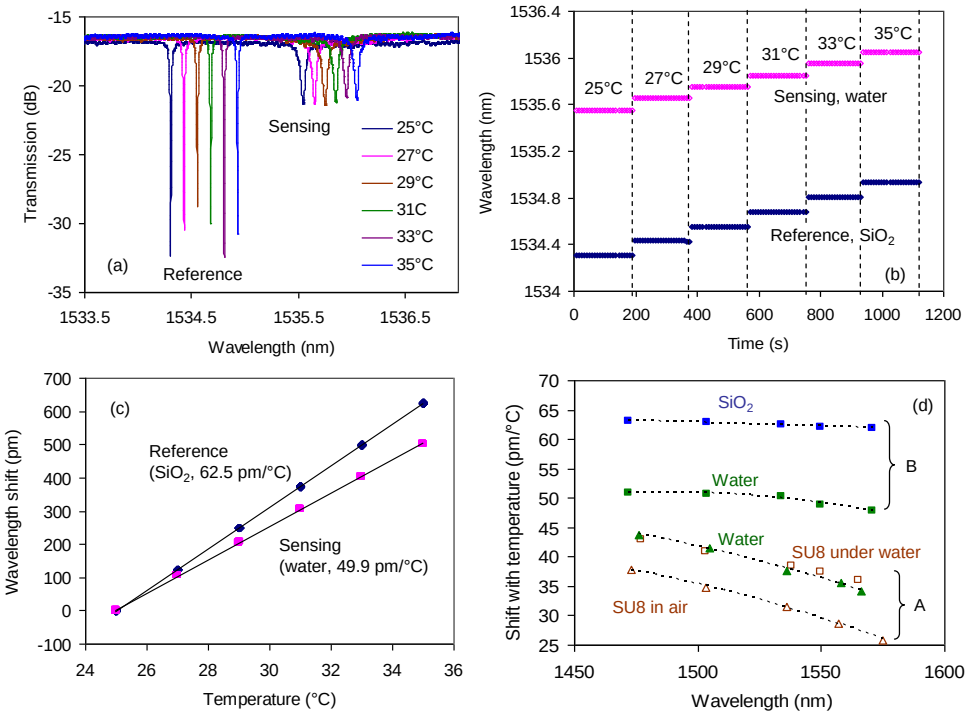

Fig. 2. (a) Transmission spectra of a reference (protected by SiO_2) and a sensing (in water) resonator from a type B sample at several steady-state temperatures with water in the fluidic channel. (b) Repeated measurements of the resonance wavelength. (c) Resonance wavelength shift as a function of temperature for data shown in (b). The slopes indicate the values of $\partial\lambda/\partial T$ for this wavelength range. (d) The values of $\partial\lambda/\partial T$ as a function of wavelength for type A and B samples with the reference resonator under different protective claddings. The lines are there to guide the eye.

Table 1: Measured and simulated temperature dependence of the resonance wavelength $\partial\lambda/\partial T$ and group index n_g for the sensing and reference resonators at λ ~1550 nm. Cross-sectional dimensions listed below and the material parameters listed in Table 2 are used for the simulations.

Sample type (Cross-section) [Reference resonator cladding]	Resonator cladding	Measured		Simulated	
		$\partial\lambda/\partial T$ (pm/°C)	n_g	$\partial\lambda/\partial T$ (pm/°C)	n_g
Type A (450 nm × 240 nm) [SU8 protective cladding]	Air (sensing)	52.6	4.37	53.6	4.34
	Water (sensing)	35.1	4.36	34.9	4.18
	SU8 under water (reference)	36.3	4.10	–	–
	SU8 in air (reference)	29.7	4.06	31.4	4.03
Type B (450 nm × 260 nm) [SiO_2 protective cladding]	Air (sensing)	60.6	4.66	64.2	4.91
	Water (sensing)	48.9	4.55	46.7	4.68
	SiO_2 (reference)	62.1	4.43	63.2	4.54

#133293 - $15.00 USD Received 11 Aug 2010; revised 6 Oct 2010; accepted 6 Oct 2010; published 13 Oct 2010

Table 2: Material properties of the waveguide core and claddings. The numbers in brackets [ ] indicate the references. The refractive index of SU8 is measured using ellipsometry.

Material	Index at $\lambda = 1550$ nm	Material dispersion (λ in μm)	TO constant (1/°C)
Silicon	3.476	$n = 3.4839 - 0.106(\lambda - 1.47) + 0.0872(\lambda - 1.47)^2$ [24]	1.86×10^{-4} [25]
SiO_2	1.444	$n = 1.445 - 0.012(\lambda - 1.47) - 0.0017(\lambda - 1.47)^2$ [24]	0.15×10^{-4} [20]
SU8 polymer	1.575	$n = 1.5753 - 0.003(\lambda - 1.47) + 0.0028(\lambda - 1.47)^2$	-1.0×10^{-4} [20]
Water	1.325	$n = 1.3256 - 0.0019(\lambda - 1.47) + 0.0017(\lambda - 1.47)^2$ [26]	-1.2×10^{-4} [26]

Figure 3(a) shows the electric field distribution of the fundamental quasi-TM mode for a wire waveguide with water upper cladding, and Fig. 3(b) shows the field line profiles across the center of the waveguide in the vertical direction (dashed line in Fig. 3(a)) for waveguides with SU8 and water upper cladding, respectively. A large fraction of the optical field resides in the upper cladding, therefore the cladding material TO constant strongly affects $\partial\lambda/\partial T$. For example, the negative TO constants of water and SU8 result in a reduced $\partial\lambda/\partial T$ compared to that for a waveguide in air (see Table 1). The refractive index of the upper cladding and waveguide cross-section size both affect the modal power fraction in the constituent waveguide materials, consequently influencing $\partial\lambda/\partial T$. As shown in Fig. 3(b), there is a slightly larger fraction of the field in the SU8 cladding layer compared that in water, due to a smaller index contrast between SU8 and Si. As a result, $\partial\lambda/\partial T$ is lower for the SU8 covered waveguide (see Table 1) even though SU8 and water have comparable TO constants. The lower values of $\partial\lambda/\partial T$ and n_g for sample A as compared to B when they are in the same cladding can be attributed to a smaller waveguide cross-section in sample A.

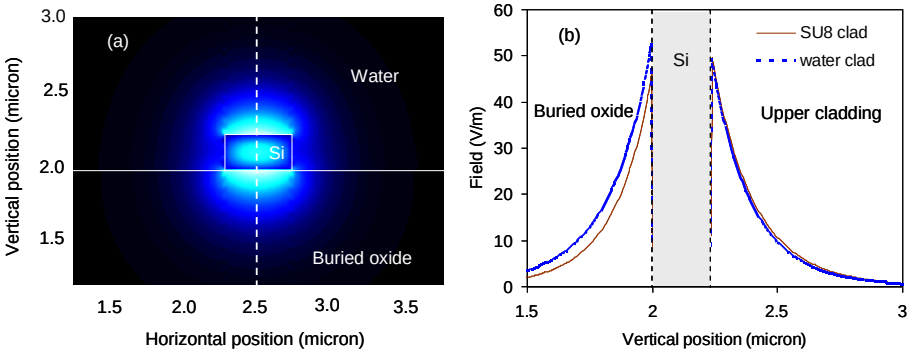

Fig. 3. (a) Modal electric field profile of a SOI waveguide with a 450 nm × 238 nm cross-section immersed in water. (b) Modal field line profile across the dashed line in (a), for waveguides with SU8 and water upper cladding, respectively.

As the operating wavelength increases, the optical field confinement in the silicon core decreases. Since silicon has the largest TO constant among the materials concerned here, the values of $\partial\lambda/\partial T$ decrease with λ for all claddings, which is experimentally observed as shown in Fig. 2d. For example, $(\partial\lambda/\partial T)_{water}$ for sample B changes from 51 pm/°C to 47 pm/°C when λ changes from 1470 nm to 1570 nm. We also found that $\partial\lambda/\partial T$ for a resonator with SU8 upper cladding changes depending on if the sample is exposed to air or immersed in water, but the measurements are reproducible under each condition. The reason for this will be discussed in the following section.

#133293 - $15.00 USD Received 11 Aug 2010; revised 6 Oct 2010; accepted 6 Oct 2010; published 13 Oct 2010

3. Real-time temperature-induced resonance shifts and their cancellation

When the sensing and reference rings are at the same temperature and there are no other factors contributing to the resonance wavelength shifts except surface adsorption ($\Delta\lambda^{0}_{sensing}$) and temperature changes (*ΔT)*, the measured total shifts for the sensing ($\Delta\lambda^{'}_{sensing}$) and reference ($\Delta\lambda^{'}_{ref}$) resonators can be expressed as:

$$\Delta\lambda^{'}_{sensing} = \Delta\lambda^{0}_{sensing} + \Delta\lambda^{T}_{sensing} = \Delta\lambda^{0}_{sensing} + (\partial\lambda/\partial T)_{sensing}\Delta T \quad (2a)$$

$$\Delta\lambda^{'}_{ref} = \Delta\lambda^{T}_{ref} = (\partial\lambda/\partial T)_{ref}\Delta T \quad (2b)$$

By combining Eq. (2)a) and (2b) to eliminate *ΔT*, the desired sensing signal $\Delta\lambda^{0}_{sensing}$ solely caused by the surface adsorption can be obtained as:

$$\Delta\lambda^{0}_{sensing} = \Delta\lambda^{'}_{sensing} - \frac{(\partial\lambda/\partial T)_{sensing}}{(\partial\lambda/\partial T)_{ref}}\Delta\lambda^{T}_{ref} \quad (3)$$

The values of $\partial\lambda/\partial$T can be calibrated under steady-state conditions, assuming that these values represent the case of real time sensing measurements. Since the rate of temperature change is generally slow in biosensing (> 1 s), we found that this is a valid assumption. Since $\partial\lambda/\partial$T is a constant within the relevant temperature range, the knowledge of the operating temperature is not required, regardless of the difference in $\partial\lambda/\partial$T between the reference and sensing rings. As described in section 2, $\partial\lambda/\partial$T shows a significant decrease with λ. However, the ratio between $(\partial\lambda/\partial T)_{sensing}$ and $(\partial\lambda/\partial T)_{ref}$ only weakly depends on wavelength. For example, $(\partial\lambda/\partial T)_{water}/(\partial\lambda/\partial T)_{oxide}$ varies from 0.81 to 0.77 over the wavelength range of 1470 nm – 1580 nm. When performing temperature drift corrections, this ratio can be considered a constant. In the following, we discuss the properties of sensing arrays with SU8 and SiO_2 claddings, and demonstrate accurate on-chip temperature drift cancellation.

3.1 Reference resonator under SU8 protective cladding

In order to use the reference resonator for on-chip temperature drift cancellation, we first need to investigate if there are other factors contributing to the reference resonator wavelength shift. As described in section 2 and listed in Table 1, $(\partial\lambda/\partial T)_{SU8}$ for a reference resonator with SU8 protective cladding changes depending on whether the sample is exposed to air or immersed in water, but the measurements are reproducible under each condition. Under steady-state condition when immersed in water, the reference and sensing rings have nearly the same $\partial\lambda/\partial$T for all wavelengths measured (1470 nm to 1580 nm), and this behavior is consistently observed for different samples with slightly different waveguide sizes. The value of $(\partial\lambda/\partial T)_{SU8}$ with only air in the channel agrees well with simulations using the measured SU8 refractive index and a TO constant of 1.0×10^{-4}/°C. These results suggest that the SU8 film properties are altered when it is immersed in water.

Repeated measurements show that apart from the changes caused by temperature fluctuation $\Delta\lambda^{T}_{ref}$, there is a slow decrease in the resonance wavelength when the device is exposed to water or other aqueous solutions, as illustrated in Fig. 4(a) for a resonator measured at a stabilized temperature of 25 °C. The drift is moderate at the beginning (~0.9 pm/min), and eventually diminishes (~0.13 pm/min after 2 hours). We speculate that this slow drift, denoted as $\Delta\lambda^{w}_{ref}$, is caused by the gradual permeation of water into the SU8 film, eventually leading to a $(\partial\lambda/\partial T)_{SU8}$ similar to that for a waveguide with water cladding. In the following, we will only discuss the case where the SU8 cladding is under an aqueous solution

#133293 - $15.00 USD Received 11 Aug 2010; revised 6 Oct 2010; accepted 6 Oct 2010; published 13 Oct 2010

as in sensing experiments. The slow blue shift as a function of time is well modeled by a polynomial fit $\Delta\lambda^{w}_{ref}$ (pm) = $-1 \times 10^{-8}\ t^3 + 5 \times 10^{-6}\ t^2 - 7 \times 10^{-4}\ t$ (time t in minutes). In sensing measurements, the total shift of the reference includes the contributions from the temperature fluctuations and the slow water permeation ($\Delta\lambda^{'}_{ref} = \Delta\lambda^{T}_{ref} + \Delta\lambda^{w}_{ref}$). By recording the fluid exposure time, the contribution from temperature changes can be isolated and corrected for.

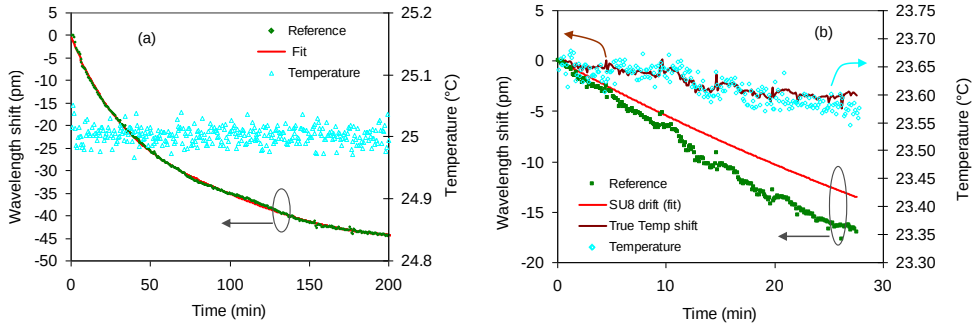

Fig. 4. (a) Reference ring resonance wavelength shift as a function of fluid exposure time for a type A sample (SU8 cladding), and the stage temperature reading when it is set at 25 °C. (b) As-measured response of the reference resonator $\Delta\lambda^{'}_{ref}$ (green symbols) for another sample exposed to the injection of 0.5%, 1% and 2% sucrose solutions (more data are shown in Fig. 5) measured without temperature control, together with the calculated SU8 drift $\Delta\lambda^{w}_{ref}$ (red line), deduced true temperature shift $\Delta\lambda^{T}_{ref}$ (brown line), and the stage temperature reading (cyan symbols).

To demonstrate temperature-induced drift cancellation, we performed real-time sensing experiments using sucrose solutions of varying concentrations. The stage was left at room temperature with the reading recorded. Analyte solutions were delivered to the reference and four sensors through a single fluidic channel at a rate of 2 mL/hour (see Fig. 1(d)). The as-measured response of the reference is shown in Fig. 4(b), while the as-measured results for all the sensors are shown in Figs. 5(a), 5(b). The measured fluid refractive index sensitivity is 135 nm/RIU (the fluid index change is 1.4×10^{-3} for 1% change in sucrose concentration), independent of the ring size as predicted by theory. The response variation between the 4 sensors is ± 1 pm for an $\Delta\lambda_R$ of 95 pm (the response to the 0.5% sucrose solution) [15]. This excellent sensing uniformity indicates good dimensional, fluidic and thermal uniformities of the sensors.

Using the polynomial fit described above and noting an initial fluid exposure time of 15 min prior to starting the sensing signal collection, we calculate $\Delta\lambda^{w}_{ref}$ and extract $\Delta\lambda^{T}_{ref}$, as shown in Fig. 4(b). The values of $\Delta\lambda^{T}_{ref}$ follows the small temperature changes closely, giving a $(\partial\lambda/\partial T)_{SU8}$ of 45 pm/°C for λ ~1550 nm, which is in reasonable agreement with the static measurement results (see Table 1). Although the calibration was done using a different chip, these results suggest that one calibration is sufficient for chips from the same batch (and therefore with similar waveguide sizes). Since the reference and sensing rings have similar $\partial\lambda/\partial T$, the compensated signal is simply $\Delta\lambda^{0}_{sensing} = \Delta\lambda^{'}_{sensing} - (\Delta\lambda^{'}_{ref} - \Delta\lambda^{W}_{ref})$. Using this procedure, the corrected sensing signal is shown in Fig. 5(c). The baselines (in DI water) for all 4 sensors are maintained to < ± 2 pm during the entire experiment. The standard deviation of the corrected baseline is 0.1 pm/min (corresponding to a fluid index variation of 7×10^{-7}), giving a resolvable resonance wavelength shift of < 0.3 pm/min.

#133293 - $15.00 USD Received 11 Aug 2010; revised 6 Oct 2010; accepted 6 Oct 2010; published 13 Oct 2010

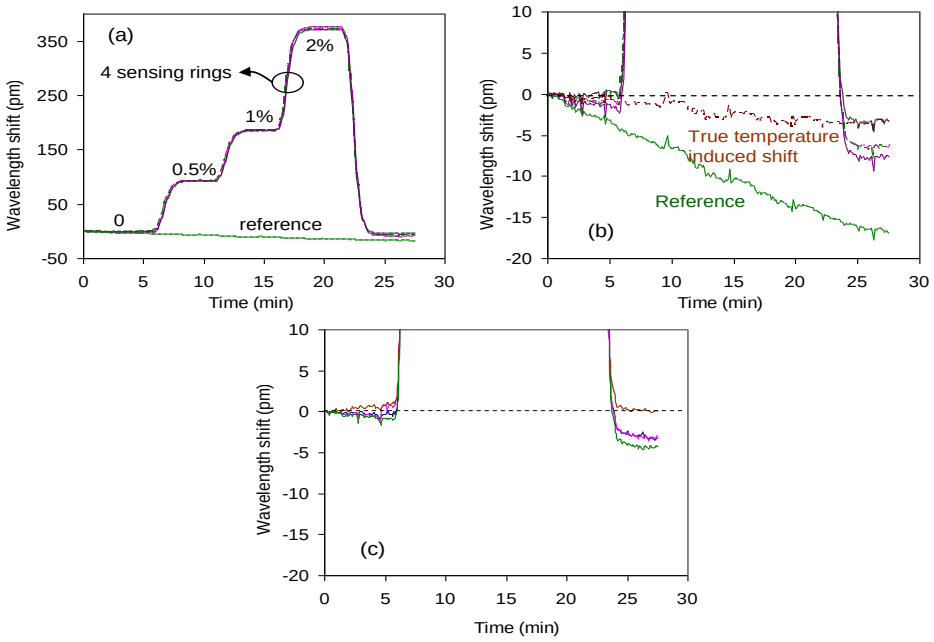

Fig. 5. (a) As-measured response of the reference and sensing ring resonators on sample A (SU8 cladding) to the injection of 0.5%, 1% and 2% sucrose solutions; (b) A close-up of (a), showing also the calculated true temperature induced shift by removing the water permeation contribution from the reference signal; (c) Corrected sensing signal.

In testing molecular binding, we use the interaction between antigen-antibody pair rabbit and anti-rabbit immunoglobulin G (IgG). After the initial silanization, rabbit IgG receptor molecules were deposited using a non-contact spotter. Details of surface preparation and multiplexed sensing results were reported previously [8,15]. Figure 6(a) shows the sensing response to 2 nM anti-rabbit IgG, between two rinsing steps in phosphate buffered saline (PBS) solution. Using the same cancellation procedure to remove water permeation and temperature induced drift, the corrected signal shows a stable value during PBS rinsing steps, while the surface adsorption is well resolved. Corrected responses to anti-rabbit IgG of 0.02, 2, 20 and 200 nM concentrations are shown in Fig. 6(b), encompassing a dynamic range of 4 orders of magnitude. These measurements were taken using a different chip for each concentration. For measurements with 20 and 200 nM protein concentrations, the surface adsorption took place rapidly and the slow drift $\Delta\lambda_{ref}^{w}$ had a negligible contribution. The estimated level of detection is 0.3 pg/mm^2, or a total bound molecular mass of 40 attograms [15]. By taking into account the effects of mass transport [8,27], molecular binding kinetic information can be obtained for even very dilute solutions.

#133293 - $15.00 USD Received 11 Aug 2010; revised 6 Oct 2010; accepted 6 Oct 2010; published 13 Oct 2010

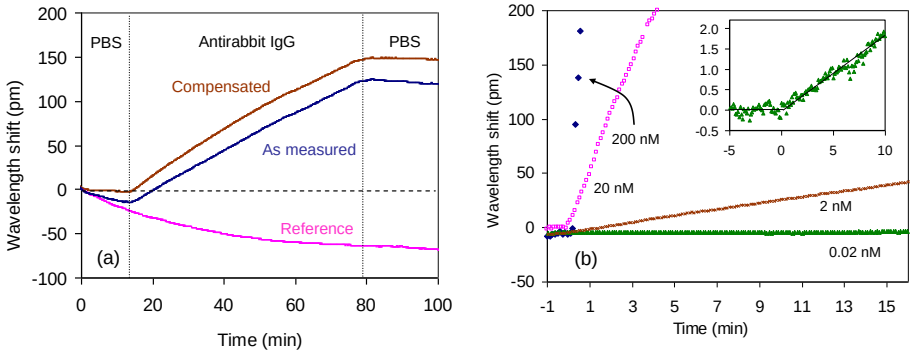

Fig. 6. (a) As-measured and corrected wavelength shifts of a sensor spotted with rabbit IgG upon exposure to 2 nM of anti-rabbit IgG solution, along with the reference ring response; (b) Corrected sensor response to varying concentrations of anti-rabbit IgG. Inset: A close up of the response to 0.02 nM IgG.

3.2 Reference resonator under SiO_2 protective cladding

To resolve minute amount of molecular binding that takes place over long time scales, contributions to wavelength shifts in the reference ring due to factors other than temperature are obviously undesirable. Oxide is a well-known passivation material and should be impermeable to most fluidic substances used in biosensing applications. As already mentioned, the fabrication process to open sensing windows in the oxide layer is more difficult due to a poor etch selectivity between Si and SiO_2. If SiO_2 cladding can provide better stability for the reference resonator, the added processing complexity is acceptable for some applications.

The stability of the reference ring on a type B sample was measured first at a stabilized temperature of 25 °C, with the sensors immersed in water inside the fluidic channel. As shown in Fig. 7, the resonances are very stable over an extended period of ~2 hours, with a wavelength scatter ≤ ± 0.5 pm (corresponding to a bulk index change of ± 4 × 10^{-6}). Compared with the results shown in Fig. 4(a), it is clear that SiO_2 provides more stable protection than SU8 for measurements involving weak molecular binding that takes place over long time scales.

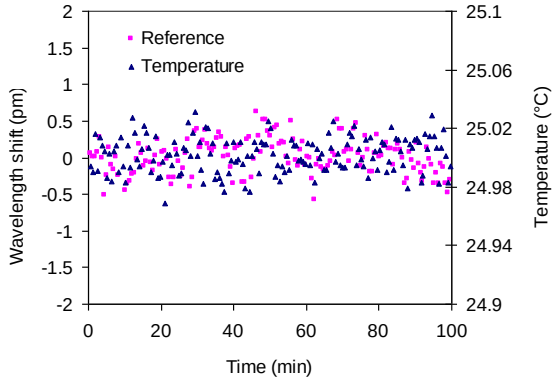

Fig. 7. Reference ring resonance wavelength shift for a type B sample (SiO_2 cladding) and the stage temperature reading as a function of time, when the temperature is set at 25°C.

The ability of real-time temperature compensation is further tested with deliberately introduced temperature fluctuations. As shown in Fig. 8, sucrose solutions of 0.1% and 0.3% (corresponding to an index increase of 1.4 × 10^{-4} and 4.2 × 10^{-4} relative to water,

#133293 - $15.00 USD Received 11 Aug 2010; revised 6 Oct 2010; accepted 6 Oct 2010; published 13 Oct 2010

respectively) were injected, separated by rinsing steps with DI water. A microscope light was switched on at 4 min and then switched off at 27 min, causing a temporary rise and fall in temperature and modifying the response of both the reference and sensing rings. As shown in Fig. 8(c), the reference ring shift closely followed the temperature change without noticeable time delay. The value of $(\partial\lambda/\partial T)_{oxide}$ is estimated to be 60.8 pm/°C (λ ~1550 nm), in good agreement with the static measurement result of 62.1 pm/°C. Taking the ratio between $(\partial\lambda/\partial T)_{water}$ and $(\partial\lambda/\partial T)_{oxide}$ as 0.8 (see Eq. (3), the corrected signal is calculated as $\Delta\lambda^{0}_{sensing} = \Delta\lambda^{'}_{sensing} - 0.8\Delta\lambda^{'}_{ref}$ and the results are shown in Fig. 8(b). The temperature induced shift is effectively removed, giving a stable base line reading with a maximum deviation of < 3 pm after 30 min.

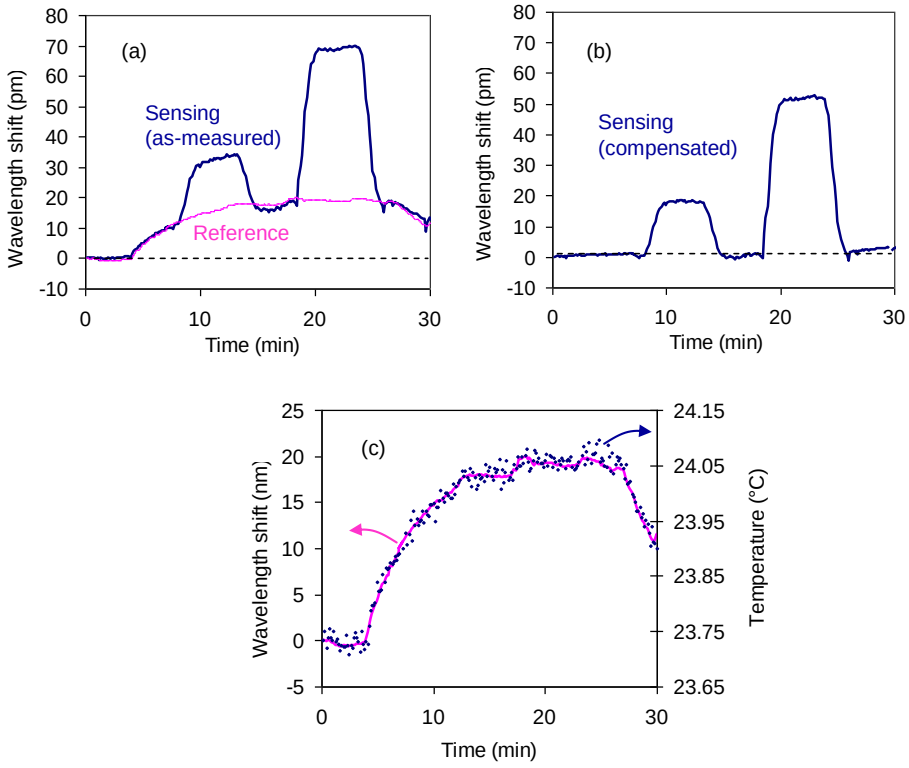

Fig. 8. (a) As-measured response of the reference and sensing ring resonators on a type B sample (oxide cladding) to the injection of 0.1% and 0.3% sucrose solutions, with DI water rinsing steps in between. A rise and fall in temperature was deliberately introduced. (b) Sensing signal with the temperature induced drift corrected; (c) Reference ring resonance wavelength shift and the stage temperature reading as a function of time.

4. Summary

The high sensitivity of a silicon photonic wire ring resonator to surface adsorbed molecules comes at the cost of a high sensitivity to changes in sensor temperature, due to the large TO constant of silicon. The ability to perform on-chip cancellation of temperature induced drifts in real-time enables high precision measurements without the need for stringent environment control. This is an important step towards developing compact and low cost resonator sensing systems.

We have systematically studied the behavior of silicon wire ring resonator sensor arrays where a reference ring, protected with a 2 μm thick upper cladding layer, is used to track

#133293 - $15.00 USD Received 11 Aug 2010; revised 6 Oct 2010; accepted 6 Oct 2010; published 13 Oct 2010

temperature changes. Two types of claddings, i.e. SU8 polymer and SiO_2, are investigated. The temperature dependence of the resonance wavelength $\partial\lambda/\partial T$ is measured under steady-state and real-time sensing conditions. We found that $\partial\lambda/\partial T$ depends on the waveguide dimensions, operating wavelength, and the cladding material TO constants. On the other hand, the ratio between $(\partial\lambda/\partial T)_{sensing}$ and $(\partial\lambda/\partial T)_{ref}$ is only weakly dependent on the wavelength and waveguide dimensions (with variations within the range of fabrication inaccuracies), and can be considered a constant when performing temperature compensation. The information of the operating temperature is not needed, simplifying instrumentation requirements. For the protective cladding thickness of 2 μm used here, real time measurements show that the reference ring tracks the temperature changes accurately with negligible time delay. Sensor arrays with a SU8 protective cladding are easy to fabricate, but the reference resonator shows a slow drift associated with the exposure to aqueous solutions. They are suitable for measurements when the sensing resonance shift takes place at a moderate rate (e.g. $\Delta\lambda_{sensing} >$ 50 pm over 10 min). Although more complex in fabrication, sensor arrays with a SiO_2 cladding show superior stability compared to that with SU8, and they are suitable for measurements involving low analyte concentrations and slow molecular binding rates.

With cancellation of the temperature-induced shifts, the sensing response exhibits high sensitivity and excellent uniformity. Bindings between complementary IgG protein pairs are monitored down to a concentration of 20 pM, demonstrating a resolvable bound molecule mass of 40 attograms (corresponding to approximately 160 IgG molecules). Reactions are measured over time periods as long as 3 hours with high stability.

Even though the experiments in this study use sensor arrays with the ring resonators coupled in series, the same compensation procedure is readily applicable to other array configurations. The only requirement is that the reference and sensing elements experience the same thermal environment, which can be achieved by placing them in the same microfluidic channel.

Acknowledgement

This work is supported in part by the Genome and Health Initiative (GHI) program of the National Research Council Canada (NRC).

#133293 - $15.00 USD Received 11 Aug 2010; revised 6 Oct 2010; accepted 6 Oct 2010; published 13 Oct 2010